Mach Number Effects on Secondary Flow Development Downstream of a Turbine Cascade

A. Perdichizzi
Professor,
Department of Mechanical Engineering,
University of Brescia,
Brescia, Italy

The results of an investigation of the three-dimensional flow downstream of a transonic turbine cascade are presented. The investigation was carried out for a wide range of Mach numbers, extending from $M_{2is}=0.2$ up to 1.55. Measurements were made in five planes at different axial locations downstream of the trailing edge (covering more than one chord length), by using a miniaturized five-hole probe especially designed for transonic flows. The results are presented in terms of local loss coefficient, vorticity, and secondary velocity plots; these plots give a detailed picture of the secondary flow development downstream of the cascade and show how flow compressibility influences the vortex configuration. As Mach number increases, the passage vortex is found to migrate toward the endwall and secondary flow effects are more confined in the endwall region. The pitchwise mass averaged loss and flow angle distributions along the blade height appear to be affected by the expansion ratio; at high Mach number both underturning and overturning angles are found to be smaller than in low velocity flows. Overall losses, vorticity, and secondary kinetic energy versus Mach number are also presented and discussed.

Introduction

In the development of modern gas turbines, significant efficiency gains have recently been obtained, and in the near future even larger improvements are expected, through increase of the firing temperature and of the overall pressure ratio. Therefore, in the design of advanced gas turbines, there is a trend toward the adoption of highly loaded turbine stages characterized by high Mach number flows. Especially in the low and medium-power range, first turbine stages have low aspect ratios and secondary flow phenomena may become important, affecting blade row performance in a significant way. Most of the published data on secondary flows refer to low-velocity flows, and limited information about secondary flow effects in high velocity cascades are available; some data were published by Sieverding and Wilputte (1981) for a nozzle cascade and by Bassi and Perdichizzi (1987) for a rotor cascade.

A great deal of experimental work has been performed recently by several authors on secondary flow in linear cascades, aiming to clarify the basic aspects of this phenomenon: Among these Gregory-Smith et al. (1988a) and Moore and Adhye (1985) have investigated the complex three-dimensional flow field evolution respectively within and downstream of linear cascades. Hodson and Dominy (1987) have shown the influence of various parameters involved in secondary flow development, such as inlet boundary layer, Reynolds number, incidence, and pitch-to-chord ratio. Moore et al. (1987) carried out turbulence measurements by hot-wire anemometer; they were able to clarify the loss generation mechanism by measuring Reynolds stresses downstream of the cascade. More recently Zunino et al. (1987, 1988) and Gregory-Smith et al. (1988b) have found that high-turbulence regions are associated with total pressure loss cores, suggesting that turbulence plays an important role in mean kinetic energy dissipation.

An aspect that has not yet been adequately investigated is the influence of Mach number; the effects of compressibility on secondary flows and related losses at the moment are not fully clear. This paper presents data on secondary flow downstream of a linear transonic cascade for different expansion ratios, ranging from subsonic incompressible flow up to supersonic flow, aiming to provide information about Mach number influence on vortex configuration, secondary loss prediction, and vorticity distribution.

Apparatus and Instrumentation

The experimental results were obtained in the C.N.P.M. (Centro Nazionale pez Ricerche sulla Propulsione e sull'Energetica, Milano) transonic wind tunnel for turbine cascades; it is a blowdown type facility with a high-pressure air storage capacity of 3100 kg and a maximum air flow rate of 12 kg/s. The test section, 400 mm wide and 50 mm high, can accept a rather large number of blades. The cascade consists of 12 blades scaled from a midspan section of a steam turbine rotor. The blade profile and the cascade geometry are presented in Fig. 1. The relatively large number of blades, together with an adjustable tailboard, contributed to minimize flow peri-

Contributed by the International Gas Turbine Institute and presented at the 34th International Gas Turbine and Aeroengine Congress and Exhibition, Toronto, Ontario, Canada, June 4–8, 1989. Manuscript received at ASME Headquarters January 1989. Paper No. 89-GT-67.

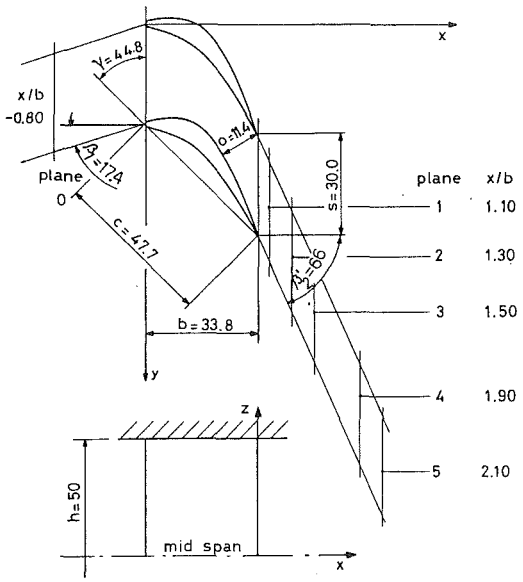

chord lenght	c = 47.7 mm.
pitch to chord	s/c = 0.63
aspect ratio	h/c = 1.05
inlet blade angle	β'_1 = 2.6 deg.
outlet blade angle	β'_2 = 66. deg.
incidence angle	i = 20. deg.
stagger angle	γ = 44.8 deg.
number of blades	z = 12

Fig. 1 Cascade geometry and measuring planes

odicity problems due to the reflection of shocks and expansion waves from the side boundary of the flow downstream of the trailing edge.

Downstream measurements were made by a miniaturized 30 deg conical pressure probe especially designed and manufactured for these tests. As can be seen from Fig. 2, the probe head has a diameter of only 1.5 mm and is 50 mm advanced from the probe stem; these characteristics were selected to minimize the blockage effects induced by the probe in the transonic regime. Meant to be used in fixed direction mode, the probe was calibrated for yaw and pitch angles ranging from −24 to +24 deg in 2-deg steps; calibration was obtained through a fully automated calibration system for Mach numbers ranging from 0.2 up to 1.8 in 0.1 steps. Downstream traverses were made in the same flow channel (the middle one) at different distances from the trailing edge, and covered 1 and 1/2 pitch so as to have a better check of the flow periodicity. The flow field within the blade passage could not be

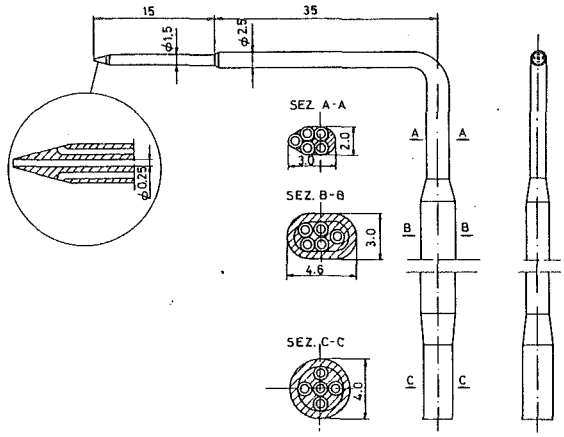

Fig. 2 Five-hole probe

Table 1 Estimated experimental uncertainties

Pitchwise position	±0.1 mm
Spanwise position	±0.1 mm
Inlet flow angle	±0.2 deg
Outlet flow angle	±0.2 deg
Stagnation pressure	±0.01 $(p_{t1}-p_{s2})$
Static pressure	±0.01 $(p_{t1}-p_{s2})$

investigated since in transonic regime the probe blockage introduces unacceptable disturbances in the flow.

Owing to the blowdown-type test facility and to the large air consumption connected to high Mach number tests, the time for a complete test on the measuring plane was severely limited. Therefore a large portion of the effort was devoted to minimizing the time required for each operation. The response time of the probe transducer system was reduced to 80 ms, locating 5 miniaturized pressure transducers just at the end of the probe stem. Probe traversing both in pitchwise and spanwise directions was achieved by stepping motors; probe position along the pitch was given by an encoder connected with the traversing carriage. Data acquisition and probe traversing were accomplished in a fully automated way by means of a microcomputer and the total time needed for a complete measuring plane (210 data points, i.e., 1900 measurements) was limited to about 150 s. Further details about the tunnel and the experimental procedure can be found in Bassi and Perdichizzi (1987).

The estimated experimental uncertainties are given in Table 1.

Generally the error in the local Mach number is estimated to be less than 0.01; for the transonic tests in planes close to

Nomenclature

a = speed of sound, m/s
b = axial chord, mm
c = chord length, mm
h = blade height, mm
H = form factor
i = incidence angle
M = Mach number
o = throat, mm
p = pressure, Pa
q = velocity, m/s
Re = qc/ν
s = pitch, mm
SKE = secondary kinetic energy
u, v, w = fluctuating velocity components, m/s
U = primary velocity, m/s
V, W = secondary velocities, m/s
x, y, z = cascade coordinates
β = flow angle
β' = blade angle
$\Delta\beta$ = secondary flow angle deviation
γ = heat capacity ratio
δ_1 = displacement thickness, mm
ζ = energy losses
θ = momentum thickness, mm
ν = dynamic viscosity
Ω = vorticity, s^{-1}

Subscripts

1 = upstream
2 = downstream (mixed out conditions)
is = isentropic
s = static
S = secondary
t = total
MS = midspan

Superscripts

$\bar{}$ = pitchwise averaged
$\bar{\bar{}}$ = pitch and spanwise averaged

Table 2 Inlet boundary layer

M_{2is}	0.32	0.50	0.72	1.02	1.23	1.38
δ_1	2.10	2.06	1.90	1.95	1.77	1.70
θ	1.61	1.68	1.51	1.56	1.37	1.37
H	1.30	1.28	1.25	1.25	1.28	1.23
$Re_2 \times 10^6$	0.35	0.59	0.84	1.23	1.55	1.61

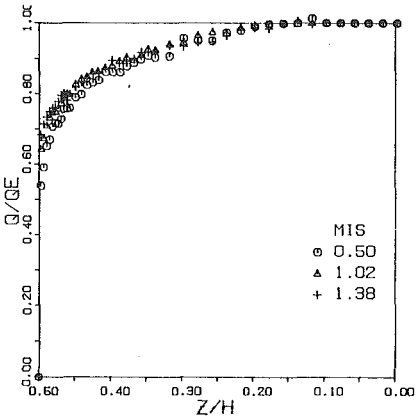

Fig. 3 Inlet boundary layer profiles

the trailing edge, larger inaccuracies occur because of probe blockage effects; also in these planes, for highly supersonic tests, probe measurements are affected by larger uncertainties, since high gradients in pitchwise direction are present. In both situations the error in the Mach number may be estimated at about 0.02–0.03, with consequent effects on the loss estimation.

Another source of inaccuracy in supersonic tests is due to the fact that, far downstream of the trailing edge, flow periodicity is more difficult to obtain and is generally worse than in the planes closer to the trailing edge; as a result much more attention had to be paid both in the setting of the tunnel and analysis of results.

Results and Discussion

Upstream Boundary Layer. The inlet boundary layer profile was determined by traversing the inlet flow at $x/b = -0.8$, by a flattened pitot probe (0.1×0.4 mm). Static pressure was obtained from wall static pressure tappings and it was assumed constant along the span. In Table 2 are presented the integral parameters of the boundary layer for the considered outlet isentropic Mach numbers; for some of these the velocity profile is shown in Fig. 3, while in Fig. 4 is presented the inlet isentropic Mach number. The boundary layer is always turbulent and the velocity profiles are almost similar.

These data show that inlet vorticity, nondimensionalized to the inlet free-stream velocity (and to a cascade reference length), is almost the same for all the cases, even if the free-stream velocity increases significantly up to the choked flow condition.

Downstream Flow Field. To show compressibility effects on secondary flows related to Mach number variation, a complete set of measurements was carried out over a wide range of expansion ratios, i.e., from $M_{2is} = 0.2$ up to 1.55 in roughly 0.2 steps. For each of the considered expansion ratios, measurements were taken in five planes downstream of the cascade, covering more than one chord from the trailing edge, as shown in Fig. 1.

Among these tests, three are presented as the most representative of different flow conditions:

$M_{2is} = 0.32$, corresponding to subsonic incompressible flow;

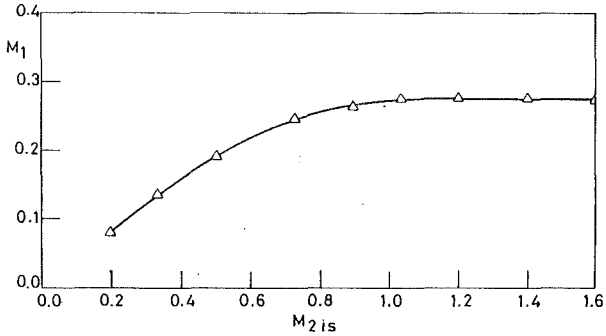

Fig. 4 Inlet Mach number

$M_{2is} = 0.92$, corresponding high subsonic/transonic flow;

$M_{2is} = 1.23$, corresponding to supersonic flow.

The results are presented in terms of kinetic energy loss coefficient, secondary velocity, and streamwise vorticity plots. The local kinetic energy loss coefficient is defined as

$$\zeta = \frac{q^2_{is(y,z)} - q^2_{2(y,z)}}{\bar{q}^2_{2isMS}} = \frac{(p_{s(y,z)}/p_{t(y,z)})^{\frac{\gamma-1}{\gamma}} - (p_{s(y,z)}/p_{t1(y,z)})^{\frac{\gamma-1}{\gamma}}}{1 - (\bar{p}_{sMS}/\bar{p}_{t1MS})^{\frac{\gamma-1}{\gamma}}}$$

The secondary velocity is defined as the projection of the velocity vector onto a plane normal to the velocity vector at midspan for a given tangential position; the velocity vector at midspan defines the primary velocity direction.

The streamwise vorticity Ω_s, i.e., the component of $\nabla x \bar{q}$ in the primary direction may be evaluated from Ω_x and Ω_y, being Ω_z perpendicular to the primary velocity direction in a linear cascade. The experimental results on each measuring plane allow a direct estimate of Ω_x, but Ω_y must be evaluated in an indirect way; following the indications of Gregory-Smith et al. (1988a), use has been made of the z component of the Crocco relation with the assumption of constant total enthalpy

$$\Omega_y = \frac{1}{q_x}\left(q_y \Omega_x + \frac{\alpha^2}{y}\frac{\partial(\ln p_t)}{\partial z}\right)$$

The vorticity values presented in the following are nondimensionalized by using inlet free-stream velocity and the blade chord.

Tests at $M_{2is} = 0.32$. The results for subsonic incompressible flow in different measuring planes are presented in Fig. 5. In the first plane downstream of the trailing edge ($x/b = 1.1$), a clear vortex configuration, typical of secondary flows, can be observed; most of the flow field is dominated by the passage vortex as indicated by the secondary velocity plot and by the large negative vorticity region on the suction side of the wake. The narrow band of positive vorticity just along the wake reveals the presence of the trailing filament and shed vortices, which, in terms of classical secondary flow theory, are related to the stretching of the vortex lines around the blades, and to the spanwise change of circulation. In the upper part of the wake. close to the endwall, there is a counterclockwise rotating flow (i.e., positive vorticity) corresponding to the corner vortex.

The loss contour plot has two peaks: a first one in the middle of the wake, where passage and shed vortices interact with each other, and the second in the corner vortex region. No loss core related to the passage vortex is found; however, there is a wide, relatively low loss region on the suction side to the wake, where low-energy fluid coming from inlet boundary layer is convected.

As the distance from the trailing edge increases, the flow field undergoes significant changes. Under the action of shear stress and turbulence the passage vortex decays, leaving an

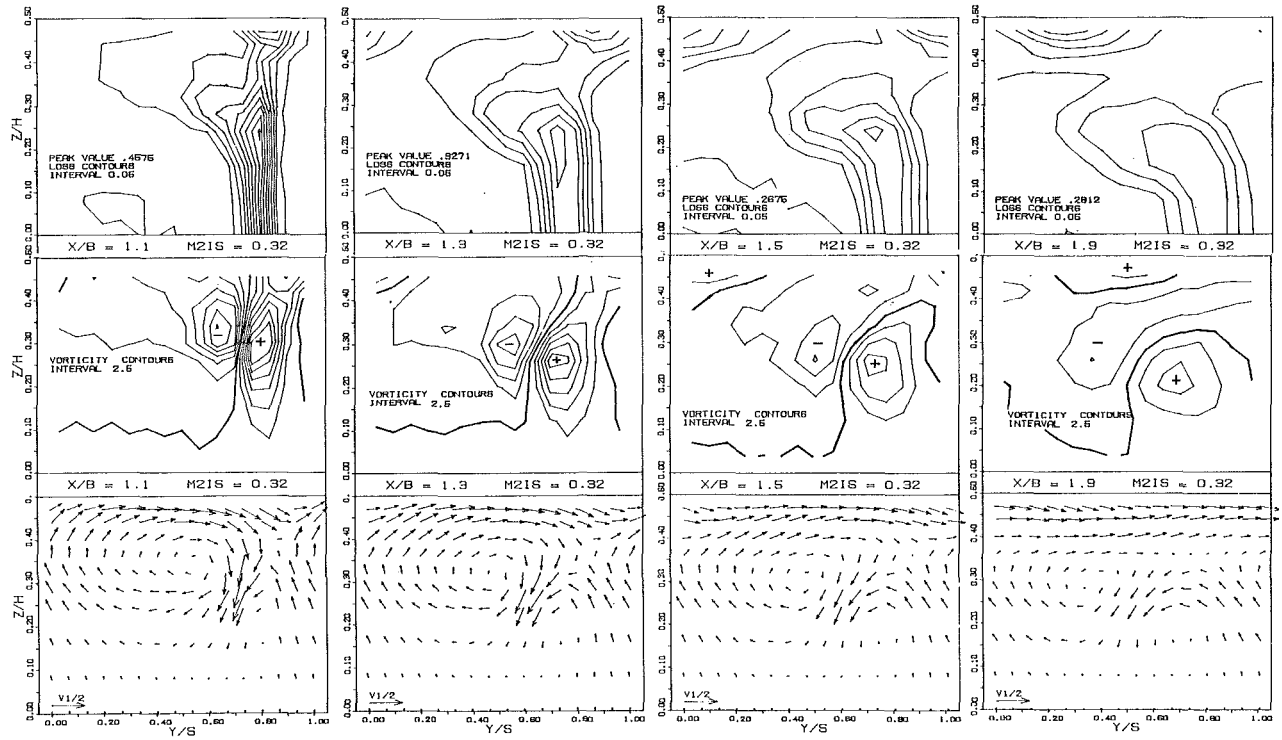

Fig. 5 Secondary velocity vectors, loss, and vorticity contours $M_{2is} = 0.32$

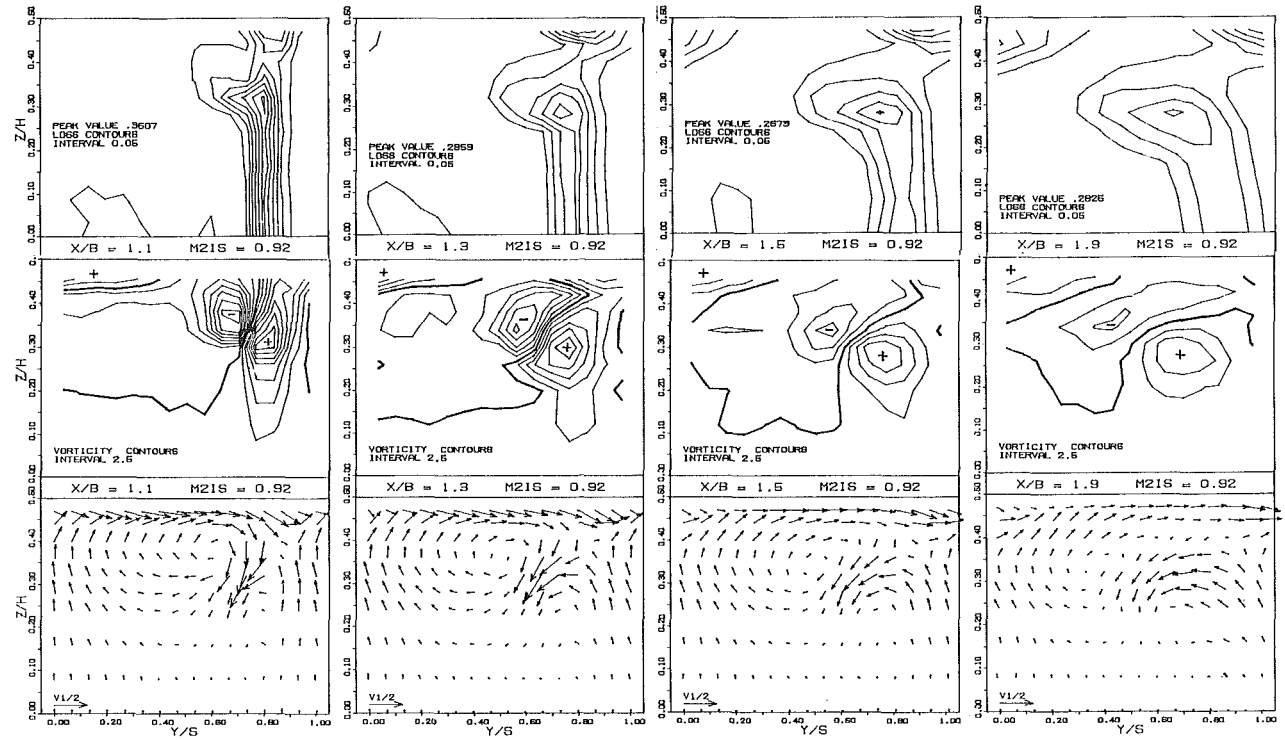

Fig. 6 Secondary velocity vectors, loss, vorticity contours for $M_{2is} = 0.92$

intense crossflow at the endwall. The trailing shed vorticity spreads over a wider zone, mostly in tangential direction; however, in the last plane, the shed vortex surpasses in intensity the passage vortex. The vorticity contours show that the passage vortex is squeezed between the shed and corner vortex, which are moving in opposite directions. Also the loss distribution changes in a significant way: Loss contours are rolled up because of the action of the passage vortex that conveys low-energy fluid toward midspan into the loss core. This loss core is found to move away from the suction side of the wake toward the middle of the channel; this is in agreement with the results of Moore and Adhye (1985). The second loss core, produced by the corner vortex and by the endwall shear stress, is convected in a pitchwise direction by the endwall crossflow and at the same time it widens considerably along the pitch and toward midspan.

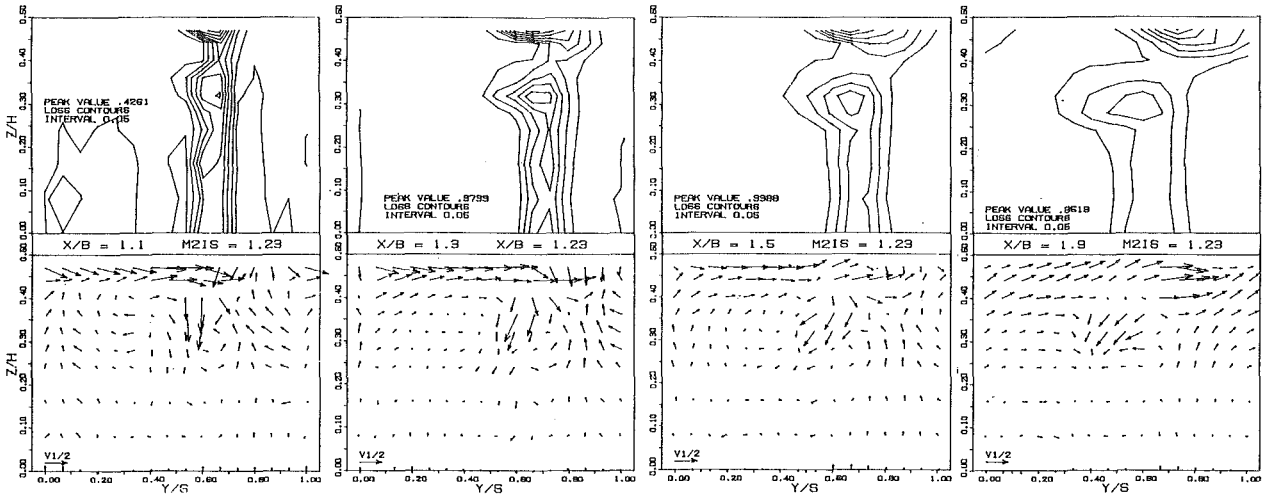

Fig. 7 Secondary velocity vectors and loss contours for $M_{2is} = 1.23$

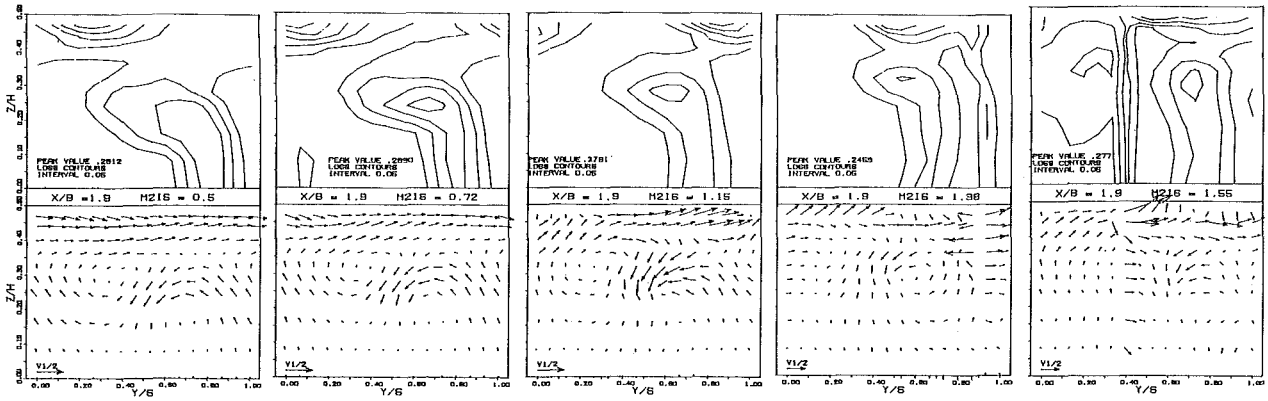

Fig. 8 Results at $x/b = 1.9$ for different M_{2is}

Tests at $M_{2is} = 0.92$. The results for high subsonic compressible flow case are presented in Fig. 6. The most interesting feature, compared to the low-velocity case, is that the passage vortex positions itself closer to the endwall and therefore the flow is two dimensional for a larger extent of the blade height. This feature is clearly shown by secondary velocities as well as by vorticity and loss contour plots. It has to be noted that only the negative vorticity core related to the passage vortex is located closer to the endwall, while the trailing shed vorticity core remains roughly in the same position as the low subsonic case. In plane 1 the vorticity distribution is similar to that of the low-velocity flow, with higher peak values (about 10–15) found both for positive and negative vorticity; as the inlet vorticity is almost the same, this means that compressibility (i.e., the larger density variation across the blade) affects the streamwise vorticity produced throughout the cascade, only slightly.

With regard to the loss distribution, a generally lower level is found, both in peak values and extent of loss region; the loss variation with the Mach number will be discussed later. The development of the flow field downstream of the cascade is similar to the previous case, but at the endwall, the corner loss core moves much less in the pitchwise direction and remains closer to the wake, because of a weaker crossflow produced by the passage vortex.

Tests at $M_{2is} = 1.23$. The secondary velocity field and the loss contour plots for the supersonic flow case are shown in Fig. 7; the vorticity distribution is not presented since its evaluation from experimental data in supersonic flows provided unrealistic results, due to an overly coarse measuring grid. In the first plane the secondary velocity field appears quite distorted, if compared to the previous cases; indeed the typical passage vortex pattern cannot be easily recognized; this is mainly caused by the high gradients (i.e., expansion and shock waves) always present in supersonic flows, especially in the trailing edge region. Moreover in the endwall region there are important effects due to the interaction of shock waves with endwall boundary layer, which produce large inward/outward secondary velocities.

Increasing the distance from the trailing edge, the mixing process reduces all the gradients, and the typical secondary flow field appears more clearly. Also the loss core on the suction side of the wake, which in plane 1 practically does not exist, grows significantly until it assumes the usual configuration. The passage vortex appears to be weak and less intense than the shed vortex. Conversely, the intensity of the corner vortex is quite large, as can be seen both from the secondary velocity and the loss contour plot; indeed the loss peak value at each measuring plane is located just in the corner vortex region. This feature is probably an effect of the three-dimensional interaction of the shock wave with endwall and blade suction side boundary layers.

In order to provide a more complete picture of the Mach number effects on the secondary flow field, a selection of results for other expansion ratios, up to very high supersonic flows ($M_{2is} = 1.55$), is presented in Fig. 8. These plots refer to plane 4, which is located at $x/b = 1.9$. As the expansion ratio is raised, the abovementioned trend of the passage vortex positioning itself closer to the endwall appears clearly. Consis-

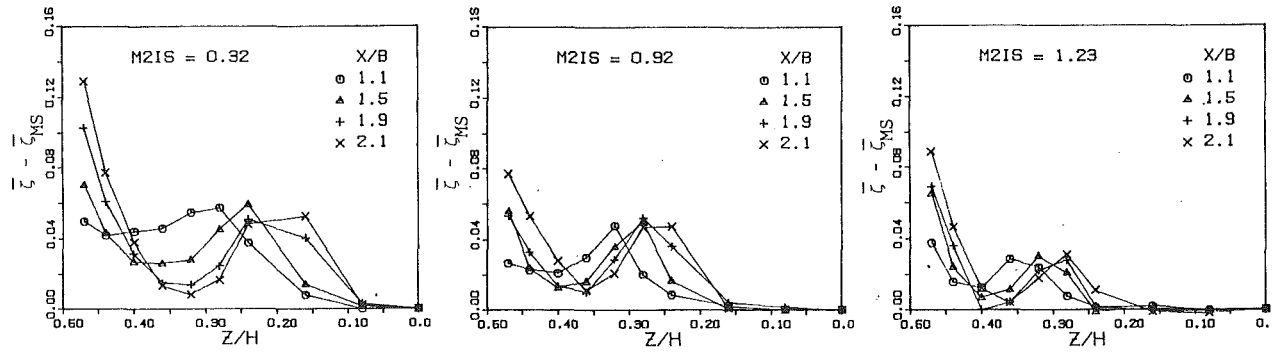

Fig. 9 Spanwise loss distribution at different planes

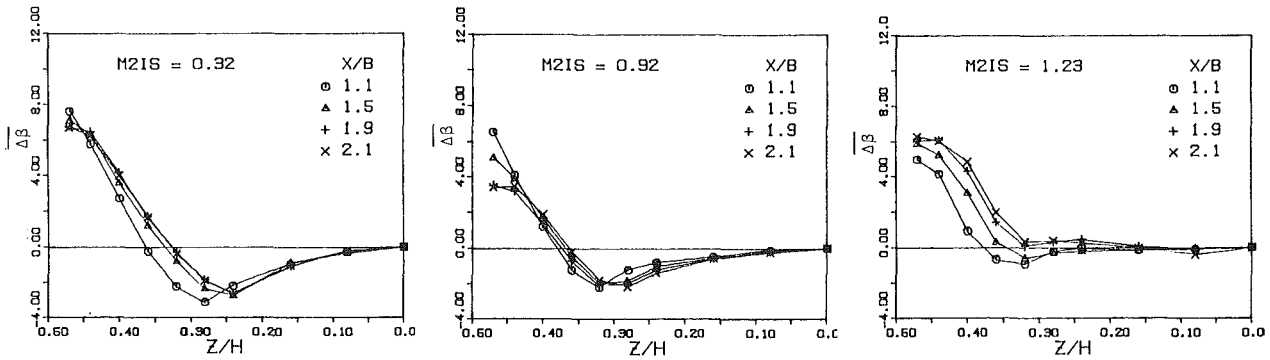

Fig. 10 Spanwise flow angle deviation at different planes

tently, the two-dimensional flow region extends progressively away from midspan and the loss core associated with the shed and passage vortices migrates toward the endwall: At $M_{2is}=0.5$ it is located at about $z/h=0.2$, while at $M_{2is}=1.38$ it is found at $z/h=0.3$.

Worthy of notice are the results for $M_{2is}=1.38$ and 1.55. They present one more loss region, just parallel to the wake, that is associated with the shock wave generated in the base pressure region. For $M_{2is}=1.38$ the shock wave bends in the tangential direction as it approaches the wall because of interaction with the boundary layer; also the secondary velocity pattern is heavily affected by the presence of the shock. For $M_{2is}=1.55$ the loss level in the endwall region is much higher since at high Mach numbers the shock loss is larger and the interaction more intense.

These results show that in supersonic flows, especially at high Mach numbers, the secondary flows in the classical sense (i.e., passage and trailing shed vortex) are less important than the three-dimensional effects connected with shock waves.

Pitch-Averaged Results. The data were mass averaged across the pitch to obtain the spanwise distributions of the loss coefficient and the flow angle deviation, defined as

$$\bar{\zeta}=\frac{\bar{q}_{2is}^2-\bar{q}_2^2}{\bar{q}_{2isMS}^2} \qquad \overline{\Delta\beta}=\bar{\beta}_2-\bar{\beta}_{2MS}$$

The results for different measuring planes are presented in Figs. 9 and 10.

As the distance from the trailing edge increases, the loss distribution undergoes significant changes and similar behavior is found for all the expansion ratios; as an example, for $M_{2is}=0.32$, at plane 1 the secondary loss is almost uniformly distributed in the region from $z/h=0.25$ up the wall; flowing downstream, low-energy fluid is accumulated toward the midspan under the rolling action of the passage vortex. At the endwall there is a significant loss increase caused by the shear stress at the wall and by the corner vortex decay. This indicates, in agreement with Sieverding and Wilputte (1981), that, once the flow is outside the blade passage, the endwall boundary layer undergoes a rapid reorganization since the low-energy fluid is no more removed from the endwall by the passage vortex.

No significant change in the deviation angle distribution except a slight migration of the underturning toward the midspan is noted downstream of the trailing edge. For $M_{2is}=0.92$, a decrease of the overturning angle can be observed close to the wall; it seems related to the larger vorticity decay downstream of the cascade occurring for compressible flows, as shown in Fig. 16.

Figures 11 and 12 show a selection of the results in plane 5 ($x/b=2.1$), showing the variation of the loss coefficient and the deviation angle versus Mach number. As the expansion ratio increases, the peak of the loss tends to move closer to the endwall, consistently with the passage vortex behavior. Beyond $M_{2is}=1.15$, i.e., after choking is reached, this trend ceases and the loss core remains almost in the same position. The peak value of the loss distribution decreases as M_{2is} rises, and for $M_{2is}=1.55$ the loss core is almost absent. In the endwall region a minimum loss value is found for transonic flows, while for higher expansion ratios a steep loss increase occurs due to the abovementioned shock wave boundary layer interaction effects.

As far as the flow angle deviation is concerned, the maximum underturning and overturning angle for the incompressible flow case are found to be about 3 and 7 deg, respectively; as the Mach number increases a progressive reduction both of the underturning and overturning angle can be observed: For $M_{2is}=1.55$ the underturning almost disappears, while the overturning reduces to about 3 deg. The reduction of the flow deviation is a consequence of the larger magnitude of primary velocities relative to the secondary ones, which takes place when the expansion ratio is increased, and especially after the choking condition is reached. At the endwall the smaller overturning is related to the larger importance assumed by the corner vortex in highly velocity flows.

These data show that the yaw angle distribution is heavily

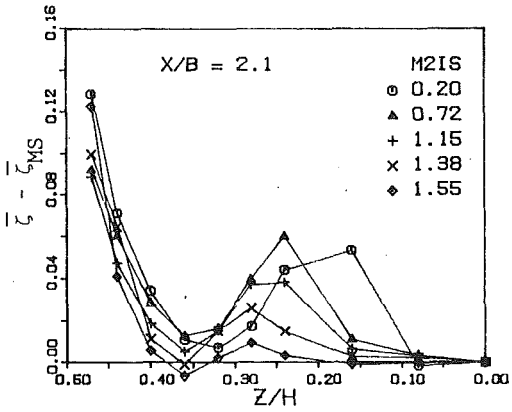

Fig. 11 Spanwise loss distribution at different M_{2is}

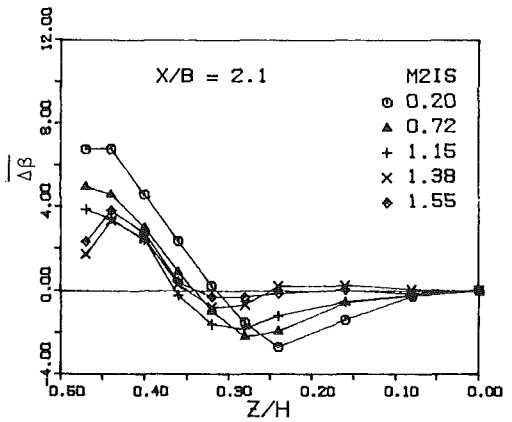

Fig. 12 Spanwise flow angle deviation at different M_{2is}

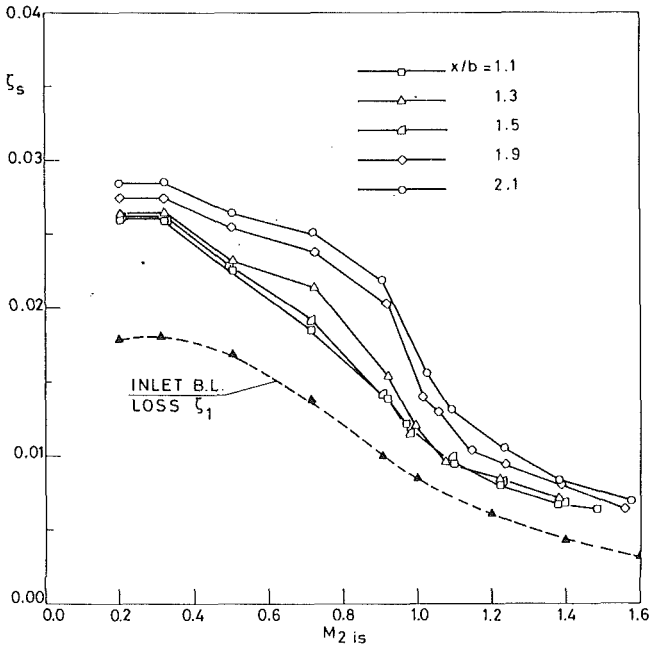

Fig. 13 Secondary losses

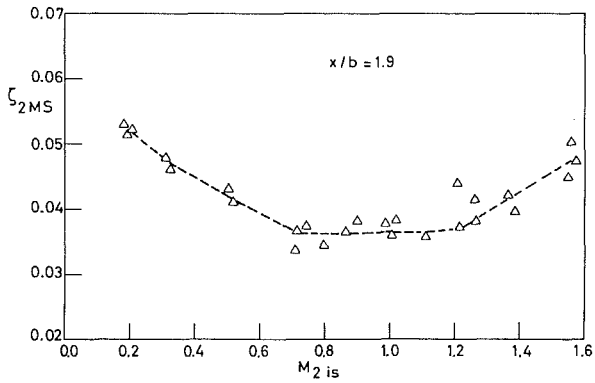

Fig. 14 Midspan loss

influenced by flow compressibility; therefore, in order to provide reliable results, a correlation for the prediction of the secondary flow angle deviation must explicitly take Mach number into account.

Area-Averaged Results. The growth of the secondary loss downstream of the cascade, versus Mach number, is shown in Fig. 13. The secondary loss was obtained by subtracting the two-dimensional loss (presented in Fig. 14) from the total loss, which was evaluated from the mass mean of the flow properties over the measuring plane. It appears that, as Mach number increases, the secondary loss undergoes a marked reduction, and for supersonic flows is is about one third of the one occurring at low Mach number. Such a reduction is mostly an effect of the huge variation in dynamic head, since the loss is referred to the outlet flow conditions. However, these results show that in transonic and supersonic flows, secondary losses, if compared to profile losses, are less important than in low subsonic flows. The results of Fig. 14 show that for $M_{2is} > 1.2$ the two-dimensional loss undergoes a significant increase; this is due to the stronger shocks generated in the base pressure region by the larger expansion occurring at the trailing edge.

To point out compressibility effects on secondary loss production, the net secondary loss produced throughout the cascade should be examined; such a loss, for all measuring planes, can be evaluated from Fig. 13 subtracting from the secondary loss the inlet loss due to the incoming boundary layer. For completeness, since usually in secondary flow analysis losses are commonly referred to inlet flow conditions, the net secondary loss in plane 5, referred to the inlet dynamic head, is also presented in Fig. 15; it should be noted that by this definition the loss is not affected by the variation of the outlet dynamic head and therefore it represents the actual energy dissipation. Both representations indicate that no appreciable variation of the net secondary loss is present up to $M_{2is} = 0.5$, i.e., in the incompressible flow range; then an important increase of energy dissipation takes place just when flow compressibility becomes significant (Fig. 15). The loss stops increasing at about $M_{2is} = 0.9$ and beyond this Mach number, i.e., in the transonic flow range, a marked reduction of the loss was found. For supersonic flows, beyond $M_{2is} = 1.2$, the loss increases again (in Fig. 13 it remains roughly constant) because of the larger importance assumed by shock wave effects.

Figure 13 shows also that in low subsonic flows, at plane 1 (i.e., at $x/b = 1.1$), most of the net secondary loss has already taken place and only a small amount is produced downstream of the trailing edge. When increasing the Mach number, a minor part of the loss is produced inside the blade passage, with the major portion generated downstream of plane 1. One can think that this feature might be related somehow to the smaller number of revolutions undergone by fluid particles involved in the passage vortex when the expansion ratio is increased.

However, it has to be pointed out that it is not clear why more energy dissipation occurs in the compressible flow range and why it is then reduced in the transonic range; an attempt to clarify this aspect was made by considering the streamwise vorticity and the secondary kinetic energy development down-

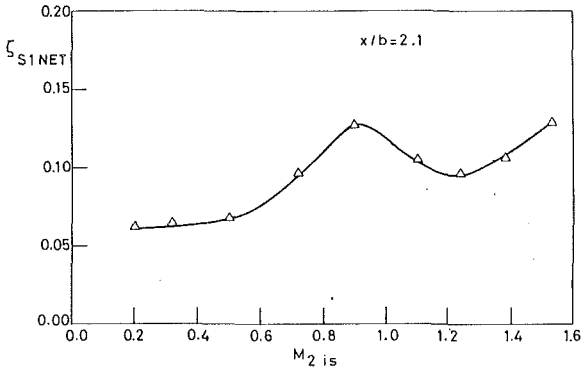

Fig. 15 Net secondary loss at $x/b = 2.1$, referred to inlet dynamic head

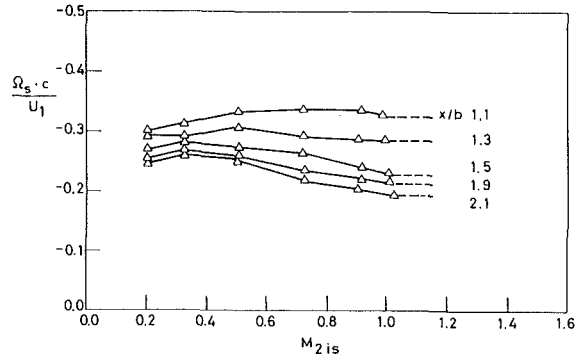

Fig. 16 Streamwise vorticity

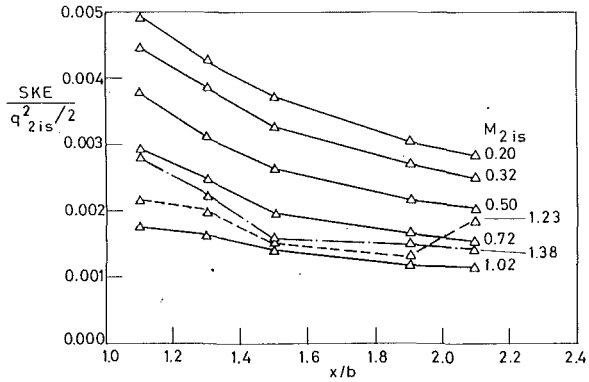

Fig. 17 Secondary kinetic energy

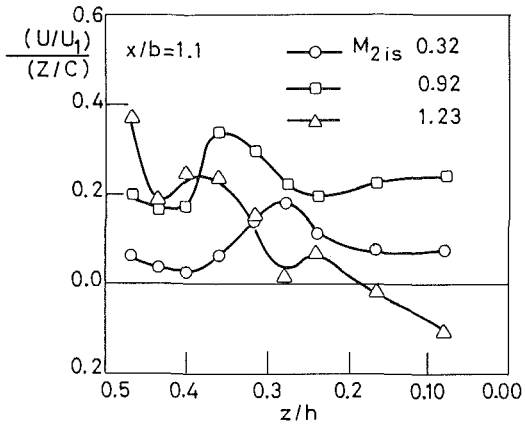

Fig. 18 Spanwise distribution of $\frac{\partial(U/U_1)}{\partial(z/c)}$

stream of the blades (Figs. 16 and 17). The secondary kinetic energy coefficient is defined as

$$\mathrm{SKE} = \int \frac{V_S^2 + W_S^2}{\bar{q}^2_{2isMS}} dydz$$

The streamwise vorticity evaluated in the first plane downstream of the trailing edge seems not to be much affected by Mach number variation; indeed slightly lower vorticities were found only in low subsonic cases. With regard to the vorticity development downstream of the cascade, it should be noted that a large vorticity decay takes place in compressible flows, while at low velocities it is much less. This trend is similar to the one observed for the net secondary loss raise (even if the rates are different); therefore a connection between loss production and vorticity decay seems to exist.

Figure 17 shows that for $M_{2is} \leq 0.3$ the SKE decay is roughly of the same order of magnitude as the loss increase between planes 1 and 5. These data are in agreement with the results of Moore and Adhye (1985) for a low-velocity cascade. For compressible flows a quite different situation occurs. The loss increase is found to be much more than the SKE decay (e.g., up to about eight times, for $M_{2is} = 1.02$). This indicates that a significant dissipation of the primary kinetic energy occurs between planes 1 and 5; part of this loss is certainly due to endwall boundary layer fluid fed into the bulk flow; however, it is the author's opinion that turbulence is mainly responsible for this loss production. Referring to the turbulent flow analysis carried out by Moore et al. (1987) in a low-velocity cascade, it seems that the opposite situation had occurred, that is mean kinetic energy could have been converted to turbulent kinetic energy through the work of deformation of the mean motion operated by Reynolds stresses. In the primary flow direction the deformation work, which contributes directly to changes in primary velocity, is expressed by

$$\frac{uu_j}{U_1^2} \frac{\partial(U/U_1)}{pt(x_j/c)}$$

This hypothesis, which could explain the higher loss production in the compressible flow cases as well as the subsequent reduction in the transonic field, is supported by the data of Fig. 18; larger values of

$$\frac{\partial(U/U_1)}{\partial(z/c)}$$

were actually found in the loss core region away from the endwall, just for $M_{2is} = 0.92$. However, it should be said that the decreasing trend noted for $0.9 < M_{1is} < 1.2$ might also be affected by the Reynolds number increase, since in these tests the variation of the Mach number involved significant Reynolds number variation (Table 3). In conclusion, a detailed investigation of the turbulent flow through hot-wire anemometry needs to be done in order to clarify the role played by turbulence in the loss production mechanism for compressible flows. This further investigation will be carried out in the near future.

Conclusions

The flow field downstream of a linear turbine cascade has been investigated over a wide range of expansion ratios. It has been found that secondary flow vortex configuration is influenced by the flow compressibility. With increasing Mach number, the passage vortex as well as the loss core on the wake suction side are found to move closer to the endwall; moreover the shed and, especially, the corner vortices tend to assume a larger importance relative to the passage vortex. In supersonic flows significant three-dimensional effects due to shock wave boundary layer interaction are superimposed on the secondary flow field. The pitch-averaged data clearly indicate a significant influence of Mach number upon the flow angle deviation dis-

tribution; smaller underturning and overturning were found at high expansion ratios.

The importance of secondary losses, compared to profile losses, is found to be diminishing as the Mach number rises. The net secondary loss increases just when flow compressibility also increases, i.e., for $M_{2is} > 0.5$, and, then, in the transonic field, undergoes a marked reduction. The data suggest that turbulence might be responsible for this trend.

Acknowledgments

The author wishes to thank Franco Tosi Industriale s.p.a., which provided the blade cascade and the permission to publish these data. The author is also grateful for the appreciated support received by C. De Ponti and G. B. Daminelli.

References

Bassi, F., and Perdichizzi, A., 1987, "Secondary Flow Development Downstream of a Transonic Cascade," *Proceedings 1987 Tokyo Gas Turbine Congress*.

Gregory-Smith, D. G., Graves, C. P., and Walsh, J. A., 1988a, "Growth of Secondary Losses and Vorticity in an Axial Turbine Cascade," ASME JOURNAL OF TURBOMACHINERY. Vol. 110, pp. 1–8.

Gregory-Smith, D. G., Walsh, J. A., and Graves, G. P., and Fulton, K. P., 1988b, "Turbulence Measurements and Secondary Flows in a Turbine Rotor Cascade," ASME JOURNAL OF TURBOMACHINERY, Vol. 110, pp. 479–485.

Hodson, H. P., and Dominy, R. G., 1987, "The Off-Design Performance of a Low-Pressure Turbine Cascade," ASME JOURNAL OF TURBOMACHINERY, Vol. 109, pp. 201–209.

Laksminarayana, B., 1975, "Effects of Inlet Temperature Gradients on Turbomachinery Performance," ASME *Journal of Engineering for Power*, Vol. 97, pp. 64–71.

Langston, L. S., Nice, M. L., and Hooper, R. M., 1977, "Three Dimensional Flow Within a Turbine Cascade Passage," ASME *Journal of Engineering for Power*, Vol. 99, pp. 21–28.

Moore, J., and Adhye, R. Y., and 1985, "Secondary Flow and Losses Downstream of a Turbine Cascade," ASME *Journal of Engineering for Gas Turbines and Power*, Vol. 107, No. 4, pp. 961–968.

Moore, J., Shaffer, D. M., and Moore, J. G., 1987, "Reynolds Stresses and Dissipation Mechanisms Downstream of a Turbine Cascade," ASME JOURNAL OF TURBOMACHINERY, Vol. 109, pp. 258–267.

Sieverding, C. M., and Wilputte, P., 1981, "Influence of Mach Number and End Wall Cooling on Secondary Flows in a Straight Nozzle Cascade," ASME *Journal of Engineering for Power*, Vol. 103, pp. 257–263.

Sieverding, C. M., 1985, "Recent Progress in the Understanding of Basic Aspects of Secondary Flow in Turbine Blade Passages," ASME *Journal of Engineering for Gas Turbines and Power*, Vol. 107, pp. 248–257.

Zunino, P., Ubaldi, M., and Satta, A., 1987, "Measurements of Secondary Flows and Turbulence in a Turbine Cascade Passage," ASME Paper No. 87-GT-132.

Zunino, P., Ubaldi, M., Satta, A., and Peisino, E., 1988, "A Comparison Between Measurements and Turbulence Models in a Turbine Cascade Passage," ASME Paper No. 88-GT-226.

APPENDIX

Blade Profile Coordinates

	X s.side	Y s.side		X p.side	Y p.side
1	0.0000	0.0000	28	33.7849	33.1481
2	0.0369	-0.2681	29	33.7396	33.3125
3	0.3118	-0.7228	30	33.6167	33.4307
4	0.7816	-0.9708	31	33.4506	33.4694
5	1.4686	-1.1336	32	33.2881	33.4177
6	2.9382	-1.4211	33	33.1749	33.2902
7	4.4068	-1.6197	34	32.3163	31.5498
8	5.8754	-1.7318	35	30.8467	28.7687
9	7.3450	-1.7584	36	29.3781	26.1495
10	8.8136	-1.6999	37	27.9095	23.6707
11	10.2823	-1.5419	38	26.4408	21.3164
12	11.7518	-1.2271	39	24.9713	19.0728
13	13.2204	-0.7450	40	23.5027	16.9148
14	14.6891	-0.0761	41	22.0340	14.6665
15	16.1577	0.8298	42	20.5645	12.8399
16	17.6272	1.9712	43	19.0958	11.2290
17	19.0958	3.3256	44	17.6272	9.7943
18	20.5645	4.9536	45	16.1577	8.5080
19	22.0340	6.9634	46	14.6891	7.3520
20	23.5027	9.5430	47	13.2204	6.3106
21	24.9713	12.5564	48	11.7518	5.3726
22	26.4408	15.6716	49	10.2823	4.5284
23	27.9095	18.8933	50	8.8136	3.7716
24	29.3781	22.2330	51	7.3450	3.0961
25	30.8467	25.7025	52	5.8754	2.4964
26	32.3163	29.3176	53	4.4068	1.9696
27	33.7634	33.0338	54	2.9382	1.5119
			55	1.4686	1.1203
			56	0.7790	0.9589
			57	0.3080	0.7192
			58	0.0355	0.2631